Multiple Model Iterative Learning Control for FES-based Stroke Rehabilitation

Junlin Zhou[1], Christopher T. Freeman[1] and William Holderbaum[2]

Abstract— Functional electrical stimulation (FES) is an effective upper limb stroke rehabilitation technology that helps patients recover lost movement by assisting functional task training. Unfortunately, current FES controllers cannot satisfy the competing demands of high accuracy, robustness to modelling error and limited set-up/identification time needed for clinical or home deployment. To address this, an estimation-based multiple model switched iterative learning control framework is proposed, combining the most successful adaptive learning features of existing FES controllers. A practical design procedure that guarantees robust performance is developed, and efficacy is established across realistic testing scenarios.

I. INTRODUCTION

One in four adults suffer a stroke in their lifetime, and 80% of survivors have impaired upper limb function [1]. Lost movement can be recovered by intensive practice of functional tasks [2] which enables the brain to receive the necessary haptic, proprioceptive and visual feedback to fuse new connections. Functional electrical stimulation (FES) facilitates task training by artificially activating muscles using a sequence of electrical pulses. It is the most popular rehabilitation technology and is supported by a substantial number of clinical studies confirming it improves arm function [3].

All commercial FES devices use open-loop control [4] due to its simple design, tuning and implementation. Similarly, the vast majority of upper limb clinical studies are either open-loop or are triggered by electromyography (EMG) [5], however resulting movements are slow and inaccurate.

A variety of closed-loop model-free FES upper limb approaches have been applied in single-session tests with healthy and stroke participants, usually to only 1 or 2 muscle groups in the arm or wrist. The most common approaches are proportional-integral-derivative (PID) position control, and proportional feedback of EMG and electroencephalographic (EEG) signals. However, tuning is time-consuming and tracking accuracy is poor due to delay and fatigue. Adding simple adaption to PID has only partially compensated for this [6]. Reinforcement learning [7] and artificial neural networks [8] have eliminated tuning, but require excessive training.

Model based upper-limb FES control has provided higher accuracy, but again has mainly focused on simple movements involving only 1 or 2 joints. Simple approaches include feedback compensation [9] and quasi-static control [10], but model identification and tuning takes 15 minutes and results in low accuracy. Model predictive [11] and optimal control [12] have improved forearm motion accuracy, but identification time and inability to handle fatigue were still substantial issues. Several sliding mode approaches have added robustness to parametric model uncertainty, but can cause discomfort, accuracy degradation, and do not provide identification details [13], [14], [15]. [16] proposed multiple model adaptive control (MMAC), applying it to isometric elbow torque. A set of models was designed, and a bank of Kalman filters computed which fitted the measured plant data best. An optimal controller designed for this model was then switched into closed-loop. MMAC is the only FES controller to be tested with multiple healthy and impaired subjects in experiments that induce full fatigue. Accuracy was high, and once the model set was designed, it could be applied to new subjects without model identification or tuning.

Iterative learning control (ILC) harnesses the repeated nature of rehabilitation training to improve accuracy, and is the only model-based upper limb approach to have been used in multiple clinical trials. Over the course of 15 years, tests with a total of 30 stroke patients have progressed to full arm reaching tasks [17] including hand and wrist motion via an FES electrode array [18]. Although accuracy has been high, identification time has become prohibitively long, and recent trials which avoided re-identification by reusing previous models yielded significantly degraded tracking accuracy.

This paper addresses the above limitations by combining the accuracy of ILC with the robustness properties of MMAC and its inability to remove identification tests. It builds on the estimation-based multiple model switched ILC (EMMILC) framework introduced in [19]. Unlike other MMAC approaches, the EMMILC performance bounds do not degrade when the number of models is increased. It develops a principled design procedure that guarantees robust stability, then verifies it on a realistic application for the first time.

II. PROBLEM STATEMENT

This section summarises the ILC design used in previous clinical applications of FES, including [17], [18].

A. ILC Framework

Consider a discrete plant operator P_p parameterised by the state-space quartet $p = (A_p, B_p, C_p, D_p)$. ILC runs over repeated trials, with index $k = 0, 1, 2, ...$ Each trial comprises N samples and the system is reset to identical initial conditions x_0. The state-space system on trial k is

$$x_k(t+1) = A_p x_k(t) + B_p u_k(t), \quad x(0) = x_0$$
$$y_k(t) = C_p x_k(t) + D_p u_k(t), \quad t = 0, 1, ..., N-1, \tag{1}$$

[1]School of Electronics and Computer Science, University of Southampton, Southampton, SO17 1BJ, UK {jz3c20,ctf1}@soton.ac.uk
[2]Department of Mathematics and Engineering, University of Reading, Reading, RG6 6AH, UK w.holderbaum@reading.ac.uk

where $u_k(t) \in \mathbb{R}^m$, $y_k(t) \in \mathbb{R}^n$ are input and output signals. The objective is to track a fixed signal y_{ref} as the trials progress, i.e. the error $e_k(t) = y_{ref}(t) - y_k(t)$ must satisfy

$$\lim_{k \to \infty} e_k(t) = 0, \quad t = 0, 1, 2, ..., N - 1. \tag{2}$$

ILC design typically 'lifts' the signals, yielding supervectors

$$u_k = [u_k(0), u_k(1), u_k(2), ..., u_k(N-1)]^\top \in \mathbb{R}^{mN},$$
$$y_k = [y_k(0), y_k(1), y_k(2), ..., y_k(N-1)]^\top \in \mathbb{R}^{nN},$$
$$y_{ref} = [y_{ref}(0), y_{ref}(1), y_{ref}(2), ..., y_{ref}(N-1)]^\top \in \mathbb{R}^{nN}. \tag{3}$$

Without loss of generality, initial condition x_0 can be absorbed into the reference so that the plant dynamics become

$$y_k = P_{\hat{p}} u_k, \tag{4}$$

where $\hat{p}$ denotes the lifted realisation of plant p, with associated matrix operator

$$P_{\hat{p}} = \begin{bmatrix} D_p & 0 & \cdots & 0 & 0 \\ C_p B_p & D_p & \cdots & 0 & 0 \\ C_p A_p B_p & C_p B_p & \cdots & 0 & 0 \\ \vdots & \vdots & \ddots & \vdots & \vdots \\ C_p A_P^{N-3} B_p & C_p A_p^{N-4} B_p & \cdots & D_p & 0 \\ C_p A_p^{N-2} B_p & C_p A_p^{N-3} B_p & \cdots & C_p B_p & D_p \end{bmatrix} \in \mathbb{R}^{mN \times nN}. \tag{5}$$

The most common ILC update form is

$$u_{k+1} = Q_{\hat{c}}(u_k + L_{\hat{c}} e_k), \tag{6}$$

where $Q_{\hat{c}} \in \mathbb{R}^{mN \times mN}$ is a robustness filter and $L_{\hat{c}} \in \mathbb{R}^{mN \times nN}$ is a learning operator. A wide variety of designs exist, see, for example, [20] for a review.

EMMILC is built on the adaptive framework of [21] shown in Fig. 1 where (u_i, y_i) represents the plant input and output ($i = 1$), external disturbances ($i = 0$) and measured signals ($i = 2$). Here unlifted plant P_p and a controller C_c operate continuously from sample to sample. To transform
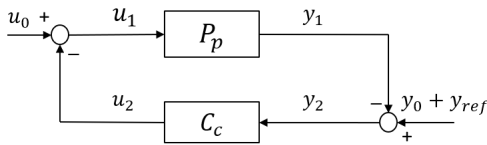
Fig. 1: Closed-loop system structure

the structure of ILC into this setting, express (4) and (6) as

$$y_1(k) = P_{\hat{p}} u_1(k), \tag{7}$$

$$u_2(k+1) = Q_{\hat{c}}(u_2(k) - L_{\hat{c}} y_2(k)), \tag{8}$$

where $u_1(k) = u_k$, $y_1(k) = y_k$, and $u_i(k) \in \mathbb{R}^{mN}$, $y_i(k) \in \mathbb{R}^{nN}$ now contain data for a whole ILC trial. Clearly (7) and (8) are both state-space systems operating in the lifted space with respective parameterisations $\hat{p} = (0, 0, 0, P_{\hat{p}})$ and $\hat{c} = (Q_{\hat{c}}, -Q_{\hat{c}}L, I, 0)$ and corresponding lifted operators $P_{\hat{p}}$ and $C_{\hat{c}}$. The standard ILC convergence condition is

$$\sigma := \|Q_{\hat{c}}(I - L_{\hat{c}} P_{\hat{p}})\| < 1. \tag{9}$$

In the case of no disturbances, i.e. $(u_0, y_0) = 0$, then

$$y_1(k) \to (I - Q_{\hat{c}}(I - L_{\hat{c}} P_{\hat{p}}))^{-1} Q_{\hat{c}} L_{\hat{c}} P_{\hat{p}} y_{ref} \text{ as } k \to \infty.$$

In particular, if $Q_{\hat{c}} = I$, then tracking objective (2) holds.

B. ILC Robust Stability

Embedding ILC in the adaptive framework of [22] immediately provides robust stability results that will be used in the EMMILC design framework. Recall that the gap metric [23] between two unlifted plant operators P_p, P_{p^*} is denoted $\delta(p, p^*)$, and characterises the distance between the two systems. It was shown in [24] that the gap metric satisfies

$$\delta(\hat{p}, \hat{p}^*) \leq \delta(p, p^*), \tag{10}$$

where $\hat{p}$, $\hat{p}^*$ are the lifted forms of plants p, p^*. Applying results from [22] yields the ILC robust stability bound:

Theorem 1: Let P_p, P_{p^*} be systems of form (1) and $C_{\hat{c}}$ be an ILC design for P_p such that condition (9) holds. Then this ILC design also stabilises plant P_{p^*} provided

$$\delta(p, p^*) < \|\Pi_{P_{\hat{p}}//C_{\hat{c}}}\|^{-1}, \tag{11}$$

where the mapping $\Pi_{P_{\hat{p}}//C_{\hat{c}}} : (u_0, y_0)^\top \mapsto (u_1, y_1)^\top$ is

$$\Pi_{P_{\hat{p}}//C_{\hat{c}}} = \begin{pmatrix} (I - C_c P_p)^{-1} & -(I - C_c P_p)^{-1} C_c \\ P_p(I - C_c P_p)^{-1} & -P_p(I - C_c P_p)^{-1} C_c \end{pmatrix}. \tag{12}$$

Furthermore, the bound satisfies

$$\|\Pi_{P_{\hat{p}}//C_{\hat{c}}}\| \leq \|(P_{\hat{p}}, I)\| \left(\frac{\|(I, P_{\hat{p}})^\top\| \|Q_{\hat{c}} L_{\hat{c}}\|}{1 - \sigma} + 1 \right). \tag{13}$$

Proof: Setting $w = (u_0, y_0 + y_{ref})$, (7), (8) give

$$[\Pi_{P_{\hat{p}}//C_{\hat{c}}} w](k) = \binom{I}{P_{\hat{p}}} \left(\sum_{i=1}^{k} \left\{ [Q_{\hat{c}}(I - L_{\hat{c}} P_{\hat{p}})]^{i-1} (Q_{\hat{c}} L_{\hat{c}} y_{ref} - Q_{\hat{c}} L_{\hat{c}}(P_{\hat{p}}, -I) w_0(k-i)) \right\} + u_0(k) \right)$$

and it follows that an upper bound on $\|\Pi_{P_{\hat{p}}//C_{\hat{c}}}\|$ is

$$\sup_{\substack{w_0(k) \in \mathbb{R}^{mN \times nN} \\ \|w_0\| \neq 0}} \frac{\left(\sum_{k=0}^{\infty} \left\| \binom{I}{P_{\hat{p}}} \sum_{i=1}^{k} [Q_{\hat{c}}(I - L_{\hat{c}} P_{\hat{p}})]^{i-1} Q_{\hat{c}} L_{\hat{c}}(-P_{\hat{p}}, I) \right. \right.}{\left(\sum_{k=0}^{\infty} \|w_0(k)\|^2 \right)^{\frac{1}{2}}}$$

$$\left. \left. \times w_0(k-i) + u_0(k) \right\|^2 \right)^{\frac{1}{2}}$$

where $w_0 = (u_0, y_0)^\top$. Setting $u_0 = 0$ and $y_0 = 0$ separately and applying relationship

$$\frac{\|\Pi_{P_{\hat{p}}//C_{\hat{c}}} w_0\|}{\|w_0\|} = \frac{\left\| \Pi_{P_{\hat{p}}//C_{\hat{c}}} \binom{u_0}{0} \right\| + \left\| \Pi_{P_{\hat{p}}//C_{\hat{c}}} \binom{0}{y_0} \right\|}{\left\| \binom{u_0}{y_0} \right\|}$$

$$\leq \left\| \Pi_{P_{\hat{p}}//C_{\hat{c}}} \Big|_{y_0=0} \right\| + \left\| \Pi_{P_{\hat{p}}//C_{\hat{c}}} \Big|_{u_0=0} \right\|$$

yields (13) after significant further manipulation. ∎

Theorem (1) provides a transparent condition for robust stability of ILC. To illustrate this, suppose P_p is a plant model and $\mathcal{U}$ is the uncertainty space specified by the designer as the set of all plants that may contain the true plant (1). Then (11) defines a gap 'ball' of plants that are stabilised by the ILC update (6). This is illustrated in Fig. 2.
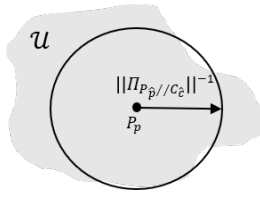
Fig. 2: Gap ball of plants stabilised by ILC update $C_{\hat{c}}$, with centre P_p, and radius $\|\Pi_{P_{\hat{p}//C_{\hat{c}}}}\|^{-1}$.

III. EMMILC FRAMEWORK

In practice ILC often has poor robustness, with a small gap radius $\|\Pi_{P_p//C_c}\|^{-1}$ generated by model P_p. EMMILC addresses this by introducing a set of 'candidate' plant models $\mathcal{P} = \{p_1, p_2, ..., p_{N_p}\}$, where each is used to design an ILC controller $\hat{c} = K(p), \forall p \in \mathcal{P}$ with K denoting the control design procedure. The set of all controllers is denoted $\mathcal{C} = \{\hat{c}_1, \hat{c}_2, \hat{c}_3, ..., \hat{c}_{N_p}\}$. Note that P_p and $C_{\hat{c}}$ are referred to by their state-space parameterisations p and $\hat{c}$. Then, gap balls of all the closed-loop systems $[P_{\hat{p}}, C_{K(p)}]$ are designed to cover the whole uncertainty set $\mathcal{U}$, as illustrated in Fig. 3.
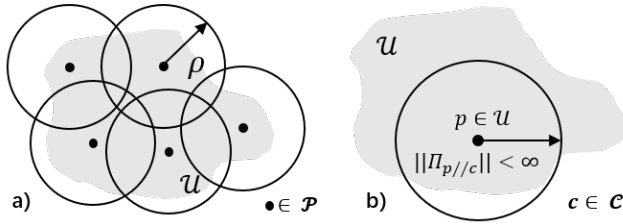
Fig. 3: a) Uncertainty set $\mathcal{U}$ covered by balls of radius ρ_p. b) Every plant $p \in \mathcal{U}$ has a stabilising controller $\hat{c} \in \mathcal{C}$.

By suitably switching between controllers, EMMILC guarantees bounded-input bounded-output stability for any true plant $P_{p^*} \in \mathcal{U}$. To decide on which ILC update to apply for each trial, a bank of Kalman estimators are designed to establish how well each plant model fits the measured data (u_2, y_2). Each estimator computes a residual, $r_{\hat{p}}$, equal to the size of the minimum disturbance necessary to explain the measurement (u_2, y_2) given that $P_{\hat{p}}$ is the true plant. Specifically, suppose $\mathcal{N}_{\hat{p}}^{[0,k]}(u_2, y_2)$ is the set of all disturbances (u_0, y_0) compatible with plant $P_{\hat{p}}$, the measured signals (u_2, y_2) and the signal connections in Fig. 1 over ILC trials $[0, k]$. Then the residual on trial k is defined as

$$r_{\hat{p}}[k] = \inf\{r \geq 0 | r = \|v_0\|, v_0 \in \mathcal{N}_{\hat{p}}^{[0,k]}(u_2, y_2)\}. \quad (14)$$

This can be calculated recursively as

$$r_{\hat{p}}[k] = \sqrt{(r_{\hat{p}}[k-1])^2 + (r_p[N-1])^2}, \quad (15)$$

where the unlifted residual over interval $[0, t]$ on trial k is

$$r_p[t] = \inf\{r \geq 0 | r = \|v_0\|, v_0 \in \mathcal{N}_p^{[0,t]}(u_2(k), y_2(k))\}. \quad (16)$$

where $\mathcal{N}_p^{[0,t]}(u_2(k), y_2(k))$ is the unlifted equivalent of $\mathcal{N}_{\hat{p}}^{[0,k]}(u_2, y_2)$ on trial k. It is shown in [25] that (16) can be

computed by the discrete-time unlifted Kalman filter using the unlifted 'along-the-trial' update

$$\tilde{x}_p(t + 1/2) = \tilde{x}_p(t) - \Sigma_p(t)C_p^\top[C_p\Sigma_p(t)C_p^\top + I]^{-1} \\ \cdot [(y_2(k))(t) + C_p\tilde{x}_p(t)] \quad (17)$$

$$\Sigma_p(t+1/2) = \Sigma_p(t) - \Sigma_p(t)C_p^\top[C_p\Sigma_p(t)C_p^\top + I]^{-1}C_p\Sigma_p(t) \quad (18)$$

$$\tilde{x}_p(t + 1) = A_p\tilde{x}_p(t + 1/2) + B_p(u_2(k))(t) \quad (19)$$

$$\Sigma_p(t + 1) = A_p\Sigma_p(t + 1/2)A_p^\top + B_pB_p^\top \quad (20)$$

with initial conditions $\Sigma_p(0)$, $\tilde{x}_p(0)$ and sample $t \in [0, N-1]$. The required $r_p[N-1]$ is then given by a weighted norm

$$r_p[N-1] = \left[\sum_{t=0}^{N-1} \|(y_2(k))(t) + C_p\tilde{x}_p(t)\|_{[C_p\Sigma_p(t)C_p^\top + I]^{-1}}^2\right]^{\frac{1}{2}}. \quad (21)$$

Computations (15),(17)-(21) incur far less load than solving (14) since they do not involve large matrices.

The ILC update corresponding to the candidate plant with the smallest residual is then used to compute the next input. The switching signals is therefore defined by

$$q(k) := \arg \min_{p \in \mathcal{P}} r_{\hat{p}}[k] \quad \forall k \in \mathbb{N} \quad (22)$$

with corresponding ILC operator $C_{K(q(k))}$. The overall EMMILC scheme is illustrated by Fig. 4.
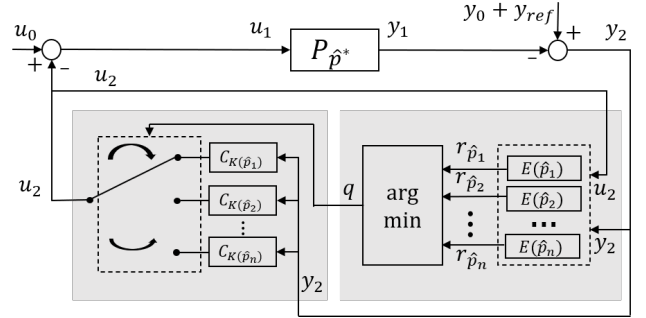
Fig. 4: EMMILC: the bank of estimators $E(.)$ defined by (17)-(21) outputs the residuals $r_{\hat{p}_1}$ to $r_{\hat{p}_n}$, the minimum residual is used to produce the switching signal q, which then selects the next ILC update.

In [19], two conditions are derived that guarantee robust performance of EMMILC when applied to an unknown plant $P_{p^*} \in \mathcal{U}$. Firstly the candidate model set $\mathcal{P}$ must satisfy

$$1) \quad \exists p \in \mathcal{P}, \quad s.t. \quad \delta(p, p^*) < \rho(\mathcal{P}, \mathcal{C}, \mathcal{U}), \quad (23)$$

where ρ is a function of the controller set $\mathcal{C}$, plant set $\mathcal{P}$ and uncertainty space $\mathcal{U}$. This criterion specifies a minimum radius of gap balls covering the uncertainty space, and hence dictates the number of estimators required. It is illustrated by Fig. 3a). Secondly, the set of controllers $\mathcal{C}$ must satisfy

$$2) \quad \exists \hat{c} \in \mathcal{C}, \quad s.t. \quad \|\Pi_{\hat{p}//\hat{c}}\| < \infty \quad \forall p \in \mathcal{U}, \quad (24)$$

which means there must exist a stabilising controller for each plant in set $\mathcal{U}$. This is illustrated in Fig. 3b).

Computing $\rho(\mathcal{P}, \mathcal{C}, \mathcal{U})$ entails a large computational burden, and is also conservative (i.e. more candidate plants are specified than required). To address this, an efficient design procedure is now developed, which does not explicitly require calculating $\rho(\mathcal{P}, \mathcal{C}, \mathcal{U})$.

Firstly, criterion (24) requires all plants in the uncertainty set $\mathcal{U}$ to be stabilised. The obvious approach to satisfy this is using the stability bound (11) to design a minimal candidate plant set $\mathcal{P}$ whose gap balls (with radius $||\Pi_{\hat{p}//K(p)}||^{-1}$) cover the uncertainty space $\mathcal{U}$. This is achieved by using Theorem 1, i.e. selecting a radius of

$$\rho_p = \gamma \|\Pi_{P_{\hat{p}}//C_{\hat{c}}}\|^{-1}, \quad (25)$$

where $\gamma = 1$. However, criterion (23) may not be satisfied. Hence the tuning parameter $0 < \gamma \le 1$ will be employed to reduce the radius of the balls. As $\gamma \to 0$, more gap balls will be included to cover the same set $\mathcal{U}$, hence (23) will always be satisfied for any ρ, avoiding the need to calculate it.

To compute the minimal set of candidate plants that cover set $\mathcal{U}$, a practical approach is to first define the largest set of plant models that resources permit, $\mathcal{H} = \{p_1, p_2, ..., p_{N_m}\}$. These should be uniformly distributed in the uncertainty space $\mathcal{U}$, then remove models that are not required. When all unnecessary models are removed, the minimum set $\mathcal{P}$ is obtained. The overall approach is stated in Algorithm 1, where the ILC controller set $\mathcal{C}$ is produced using the resulting minimum plant set. The principle is illustrated by Fig. 5.

Algorithm 1 Design Procedure

Require: ILC design procedure K, and $0 < \gamma \le 1$
Ensure: Minimal candidate plant set $\mathcal{P}$
1: Define $\mathcal{H} = \{p_1, p_2, ..., p_{N_m}\}$ as the finest grid that computational resources allow;
2: Set $S = \{0, 0, ..., 0\}$ with N_m elements, S_j denoting the jth element;
3: **for** each $i \in \{1, 2, 3, ..., N_m\}$ **do**
4:     **for** each $j \in \{1, 2, 3, ..., N_m\}$ **do**
5:       **if** $\exists a \in \{1, 2, 3, ..., N_m\}$, s.t. $S_a = 0$ **then**
6:         Design $Q_{\hat{c}_i}, L_{\hat{c}_i}$ for $\hat{c}_i = K(p_i)$, s.t. bound (13) is minimised, $||\Pi_{\hat{p}_i//K(p_i)}||^{-1}$ is maximised.
7:         **if** $\delta(\hat{p}_i, \hat{p}_j) < \gamma ||\Pi_{\hat{p}_i//K(p_i)}||^{-1}$ **then**
8:           $S_j = i$;
9:         **end if**
10:       **else**
11:         Delete repetitions from S, set $N_p = |S|$;
12:         $\mathcal{P} = \{P_{p_{S_1}}, P_{p_{S_2}}, ..., P_{p_{S_{N_p}}}\}$; Exit loops;
13:       **end if**
14:     **end for**
15: **end for**
16: Return $\mathcal{P}$.

IV. PRACTICAL VERIFICATION

In this section EMMILC is compared with the standard ILC approach used in FES based rehabilitation (a fixed controller) using a clinically relevant application. The tracking performance will be measured with different values of γ.
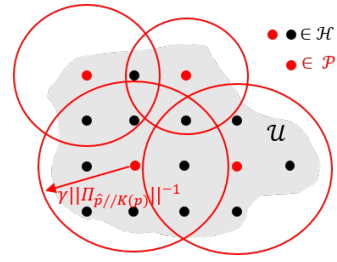
Fig. 5: The black plant models are not needed and removed from the initial plant set $\mathcal{H}$. The remaining red plants form the minimal candidate plant set $\mathcal{P}$, which still covers $\mathcal{U}$.

A. Model and Controller Design

From [26], an accurate model of wrist dynamics that is widely used for FES control design is given by

$$P_p(s) = h_{IRC} \cdot \frac{\omega_n^2}{s^2 + 2\omega_n s + \omega_n^2} \cdot \frac{1}{I_s s^2 + B_s s + K_s}, \quad (26)$$

where physiological parameters $h_{IRC}, \omega_n, I_s, B_s$ and K_s denote the isometric recruitment curve (IRC) constant, natural frequency, inertia, damping and stiffness, respectively, and vary from patient to patient. The input to this model is the FES pulsewidth, and the output is the wrist angle. Nominal wrist parameter are taken from practical data measured in [26], [27], [28] and [29], and are listed in Table I. Because stiffness and inertia vary most among individuals, this simulation only considers their ranges.

TABLE I: Values of wrist parameters.

Symbol	Nominal value	Uncertainty range	Unit
h_{IRC}	0.0117	N/A	N/A
ω_n	9.4248	N/A	rads/s
K_s	1.62	$0.62 \sim 3.24$	Nm/rad
B_s	0.128	N/A	Nms/rad
I_s	0.0045	$0.0007 \sim 0.00612$	Nms^2/rad

The reference trajectory is selected to produce $60°$ wrist extension corresponding to a grasp and release task. A sampling time of 0.025 seconds ($40Hz$) and a duration of 7.5 seconds are also chosen to match existing clinical implementations, yielding $N = 300$ samples. The model uncertainty set $\mathcal{U}$ comprises the parametric uncertainties defined in Table I.

The inverse ILC update with step size $\beta = 1$ is employed due to its rapid convergence and prior tremor implementation [30], hence producing $L_{\hat{c}} = P_{\hat{p}}^{-1}$. A 10th order zero-phase low-pass filter with cut-off frequency $5Hz$ is established and lifted using (5) to produce a robustness filter $Q_{\hat{c}}$, in order to satisfy the design protocol in Algorithm 1. The ILC update $C_{\hat{c}}, \hat{c} = K(p)$ is hence given by

$$u_2(k+1) = Q_{\hat{c}}[u_2(k) - P_{\hat{p}}^{-1} y_2(k)], \quad \forall p \in \mathcal{H}. \quad (27)$$

To design the candidate model set, Algorithm 1 is now implemented using tuning parameter $\gamma = 1$. This is chosen to

establish whether a minimum candidate plant set can provide satisfactory performance. Within Algorithm 1, $N_m = 100$ is selected for the initial plant set $\mathcal{H}$ since it takes approximately one hour to compute the minimum plant set, which is deemed acceptable for each implementation.

After implementation, the output of Algorithm 1 is a minimal candidate plant set $\mathcal{P} = \{p_1, p_2, ..., p_{N_p}\}$ comprising $N_p = 36$ plants (64 having been removed). The candidate controller set $\mathcal{C} = \{\hat{c}_1, \hat{c}_2, \hat{c}_3, ..., \hat{c}_{N_p}\}$ contains 36 ILC controllers, each corresponding to a plant $p \in \mathcal{P}$.

B. Evaluation of Tracking Performance

To evaluate the effect of EMMILC, it will be compared to standard ILC, with the latter designed using a nominal model, denoted p^f, whose wrist parameters are taken from Table I. Meanwhile, the true plant p^* has parameters $K_s = 3.24$, $I_s = 7 \times 10^{-4}$, $B_s = 0.1280$, $h_{IRC} = 0.0117$ and $\omega_n = 9.4248$. Here the true value of K_s is increased and I_s is decreased compared to the nominal parameters in Table I due to isometric effort [31], in order to simulate a moderately fatigued wrist. This true plant is not one of those in the candidate model set $\mathcal{P}$. To replicate experimental conditions, the external disturbances (u_0, y_0) in Fig. 1 are chosen as white noise with a signal-to-noise ratio of 8%.

First standard ILC is applied with a fixed controller $K(p^f)$ designed using the nominal model P_{p^f}. After 6 ILC trials, the tracking results show that the error norm rapidly diverges, and eigenvalues of the error evolution $Q_{\hat{c}}(I - P_{\hat{p}^f}^{-1} P_{\hat{p}^*})$ confirm that the closed-loop system $[P_{\hat{p}^*}, C_{K(p^f)}]$ is indeed unstable. The failure of standard ILC hence motivates the application of EMMILC.

The final trial tracking performance of EMMILC is shown by Fig. 6b). The results show the error norm rapidly converges to a sufficiently small value with a selected controller switched into the closed-loop system after the first ILC trial. The switching signal is shown by Fig. 6a, where the plant p_{75} has the lowest residual, and the corresponding controller $C_{K(p_{75})}$ is switched into closed loop on the 2nd trial to form the stable closed-loop system $[P_{\hat{p}^*}, C_{K(p_{75})}]$. Eigenvalues also confirm that this closed-loop system is stable.
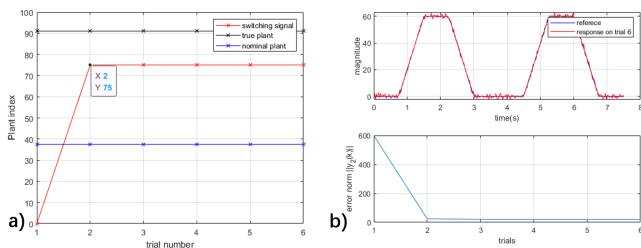
Fig. 6: a) Switching signal settles at p_{75} on trial 2. b) Top plot shows the EMMILC tracking output on trial 6. Bottom plot shows the error norm $\|y_2(k)\|$ for each trial k.

In order to evaluate EMMILC on a realistic case, a severely fatigued wrist is also simulated by increasing the stiffness and reducing the inertia to obtain $K_s = 12.96$ and

$I_s = 1.75 \times 10^{-4}$. These values are actually outside the set $\mathcal{U}$ to further test the capability of EMMILC. The value of γ in Algorithm 1 is reduced to increase the number of candidate plants N_p, hence guaranteeing stability and robust performance in the presence of moderate and severe fatigue. To quantify the performance, the accuracy index

$$D = \left(1 - \frac{\|e_6\|}{\|e_1\|}\right) \times 100\%. \qquad (28)$$

is used, since it captures both convergence speed and final tracking accuracy. Different values of γ are tested, and the tracking accuracy for each case is shown in Table II.

TABLE II: Accuracy after 6 trials for standard ILC and different γ in the cases of NF (no fatigue) for $[P_{p^f}, C_{K(p^f)}]$, MF (moderate fatigue) and SF (severe fatigue). A red D value means the error is diverging.

D value	NF	MF	SF	N_p
standard ILC	96.47%	94.73%	46.57%	N/A
$\gamma = 1$	96.48%	96.42%	95.83%	36
$\gamma = 0.5$	96.62%	96.55%	96.24%	62
$\gamma = 0.25$	96.71%	96.68%	96.46%	84

The results confirm that the standard ILC update cannot stabilise either the moderately or the severely fatigued wrist. However, EMMILC with the original plant set of 36 candidate plants provides accurate tracking. Adding more candidate plants slightly improves the performance at the expense of computational burden, but is unnecessary unless very high accuracy is required. If the patient's wrist becomes severely fatigued during intensive task practice, the accuracy decreases and the closed loop system becomes unstable with $\gamma = 1$ due to the unsatisfied stability criterion (23). In this case, reducing the value of γ addresses this problem by increasing the number of candidate plants until $N_p = 62$. Eventually, the most accurate result is obtained with $D = 96.71\%$ when $\gamma = 1$ before the occurrence of fatigue.

During intensive training tasks, moderate fatigue occurs first and is followed by severe fatigue. To evaluate the efficacy of EMMILC in a realistic training scenario, it is assumed that there is no fatigue on trial $k = 1, 2$, then moderate fatigue occurs on trial $k = 3$ and progresses to severe fatigue on trials $k = 4, 5, 6$. This overall process of sequentially fatiguing the wrist yields the tracking performance shown in Fig. 7b), with corresponding switching signals shown in Fig. 7a). The diverging errors show that the standard ILC and the EMMILC with $\gamma = 1$ cannot compensate for the fatigue which sequentially changes in a practical training scenario. This is also addressed by reducing γ from 1 to 0.5, which increases the number of candidate plants N_p from 36 to 62. The switching signals in Fig. 7a) do not change when moderate fatigue progresses to severe fatigue. However, reducing γ then satisfies stability criterion (23), which demonstrates the utility of Algorithm 1.

V. CONCLUSION

This paper addresses limitations of FES-based stroke rehabilitation by introducing an adaptive multiple model ILC
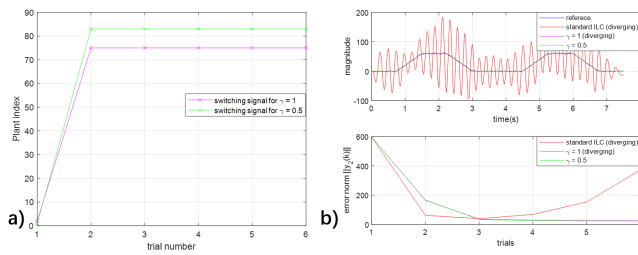
Fig. 7: a) Switching signal for $\gamma = 1$ and $\gamma = 0.5$. There is no switch when severe fatigue occurs because it is outside the uncertainty set $\mathcal{U}$. b) Top plot shows the tracking output on trial 6. Bottom plot shows the error norm $\|y_2(k)\|$.

approach. A computationally efficient design procedure is proposed based on gap metric stability bounds, and enables guaranteed stability for any true plant within an uncertainty space specified by the designer. A case study confirmed the EMMILC framework's efficacy in realistic clinical conditions. Future work will evaluate EMMILC experimentally with stroke patients, first using single-pad electrodes and then multi-electrode FES arrays to control hand, wrist and arm motion. The ultimate aim will be to highly assist movement while eliminating model identification and tuning.

REFERENCES

[1] K. S. Hayward, S. F. Kramer, V. Thijs, and et.al., "A systematic review protocol of timing, efficacy and cost effectiveness of upper limb therapy for motor recovery post-stroke," *Systematic reviews*, vol. 8, no. 1, p. 187, 2019.
[2] B. H. Dobkin, "Strategies for stroke rehabilitation," *the Lancet Neurology*, vol. 3, no. 9, pp. 528–536, 2004.
[3] O. A. Howlett, N. A. Lannin, L. Ada, and C. McKinstry, "Functional electrical stimulation improves activity after stroke: A systematic review with meta-analysis," *Archives of Physical Medicine and Rehabilitation*, vol. 96, no. 5, pp. 934–943, 2015.
[4] D. B. Popović, "Advances in functional electrical stimulation (fes)," *Journal of Electromyography and Kinesiology*, vol. 24, no. 6, pp. 795–802, 2014.
[5] M. G. H. Kristensen, H. Busk, and T. Wienecke, "Neuromuscular electrical stimulation improves activities of daily living post stroke: A systematic review and meta-analysis," *Journal of Electromyography and Kinesiology*, vol. 4, no. 1, p. 100167, 2022.
[6] P. Paz, T. R. Oliveira, A. V. Pino, and A. P. Fontana, "Model-free neuromuscular electrical stimulation by stochastic extremum seeking," *in IEEE Transactions on Control Systems Technology*, vol. 28, no. 1, pp. 238–253, 2020.
[7] A. Koushki, M. Karami, M. Abbasi, and et.al., "Deep reinforcement learning control of elbow motion under functional electrical stimulation," in *2021 9th RSI International Conference on Robotics and Mechatronics (ICRoM)*, pp. 132–137, 2021.
[8] F. Resquín, J. Gonzalez-Vargas, J. Ibáñez, and et.al., "Feedback error learning controller for functional electrical stimulation assistance in a hybrid robotic system for reaching rehabilitation," *European journal of translational myology*, vol. 26, no. 3, pp. 255–261, 2016.
[9] R. S. Razavian, B. Ghannadi, N. Mehrabi, and et.al., "Feedback control of functional electrical stimulation for 2-d arm reaching movements," *IEEE Transactions on Neural Systems and Rehabilitation Engineering*, vol. 26, no. 10, pp. 2033–2043, 2018.
[10] D. N. Wolf and E. M. Schearer, "Holding static arm configurations with functional electrical stimulation: A case study," *IEEE Transactions on Neural Systems and Rehabilitation Engineering*, vol. 26, no. 10, pp. 2044–2052, 2018.
[11] D. N. Wolf and E. M. Schearer, "Trajectory optimization and model predictive control for functional electrical stimulation-controlled reaching," *IEEE Robotics and Automation Letters*, vol. 7, no. 2, pp. 3093–3098, 2022.
[12] S. Sa–e, C. T. Freeman, and K. Yang, "Iterative learning control of functional electrical stimulation in the presence of voluntary user effort," *Control Engineering Practice*, vol. 96, p. 104303, 2020.
[13] T. R. Oliveira, L. R. Costa, J. M. Y. Catunda, and et.al., "Time-scaling based sliding mode control for neuromuscular electrical stimulation under uncertain relative degrees," *Medical Engineering and Physics*, vol. 44, pp. 53–62, 2017.
[14] C. A. Rouse, A. Parikh, V. Duenas, and et.al., "Compensating for changing muscle geometry of the biceps brachii during neuromuscular electrical stimulation: A switched systems approach," in *2016 IEEE 55th Conference on Decision and Control (CDC)*, pp. 1328–1333, 2016.
[15] Q. Wu, X. Wang, F. Du, and et.al., "Modeling and position control of a therapeutic exoskeleton targeting upper extremity rehabilitation," *Proceedings of the Institution of Mechanical Engineers, Part C: Journal of Mechanical Engineering Science*, vol. 231, no. 23, pp. 4360–4373, 2017.
[16] O. Brend, C. T. Freeman, and M. French, "Multiple-model adaptive control of functional electrical stimulation," *IEEE Transactions on Control Systems Technology*, vol. 23, no. 5, pp. 1901–1913, 2015.
[17] M. Kutlu, C. T. Freeman, E. Hallewell, and et.al., "Upper-limb stroke rehabilitation using electrode-array based functional electrical stimulation with sensing and control innovations," *Medical Engineering and Physics*, vol. 38, no. 4, pp. 366–379, 2016.
[18] T. Excell, C. T. Freeman, K. Meadmore, and et.al., "Optimisation of hand posture stimulation using an electrode array and iterative learning control," *Journal of Automatic Control*, vol. 21, no. 1, pp. 1–4, 2013.
[19] C. T. Freeman and M. French, "Estimation based multiple model iterative learning control," in *2015 54th IEEE Conference on Decision and Control (CDC)*, pp. 6070–6075, 2015.
[20] D. A. Bristow, M. Tharayil, and A. G. Alleyne, "A survey of iterative learning control," *IEEE Control Systems Magazine*, vol. 26, no. 3, pp. 96–114, 2006.
[21] D. Buchstaller and M. French, "Robust stability for multiple model adaptive control: Part i—the framework," *IEEE Transactions on Automatic Control*, vol. 61, no. 3, pp. 677–692, 2016.
[22] T. T. Georgiou and M. C. Smith, "Optimal robustness in the gap metric," in *Proceedings of the 28th IEEE Conference on Decision and Control*, vol. 3, pp. 2331–2336, 1989.
[23] G. Zames and A. K. El-sakkary, "Unstable systems and feedback: The gap metric," in *roc. of the Allerton Conference*, pp. 380–385, 1980.
[24] R. S. Bradley, *The Robust Stability of Iterative Learning Control*. PhD thesis, University of Southampton, 2010.
[25] J. C. Willems, "Deterministic least squares filtering," *Journal of Econometrics*, vol. 118, no. 1-2, pp. 341–373, 2004.
[26] A. W. Peaden and S. K. Charles, "Dynamics of wrist and forearm rotations," *Journal of Biomech.*, vol. 47, no. 11, pp. 2779–2785, 2014.
[27] S. K. Charles and N. Hogan, "Stiffness, not inertial coupling, determines path curvature of wrist motions," *Journal of Neurophysiology*, vol. 107, no. 4, pp. 1230–1240, 2012.
[28] S. K. Charles and N. Hogan, "Dynamics of wrist rotations," *Journal of Biomech.*, vol. 44, no. 4, pp. 614–621, 2011.
[29] K. Park, P. H. Chang, and S. H. Kang, "In vivo estimation of human forearm and wrist dynamic properties," *IEEE Transactions on Neural Systems and Rehabilitation Engineering*, vol. 25, no. 5, pp. 436–446, 2017.
[30] Z. Zhang, B. Chu, Y. Liu, and et.al., "Wrist tremor suppression based on repetitive control with multi-muscle electrical stimulation," *IFAC-PapersOnLine*, vol. 52, no. 29, pp. 31–36, 2019.
[31] M. Lakie and L. G. Robson, "Thixotropic changes in human muscle stiffness and the effect of fatigue," *Quarterly Journal of Experimental Physiology*, vol. 73, no. 4, pp. 487–500, 1988.